Supporting Information

Self-healing Bottlebrush Polymer Networks Enabled via a Side-chain Interlocking Design

Hui Xiong[1a], Tongkui Yue[1b], Qi Wu[a], Linjun Zhang[a], Zhengtian Xie[a], Jun Liu*[b], Liqun Zhang[b] and Jinrong Wu*[a]

[1] These authors contributed equally to this work and should be considered as co-first authors

*Corresponding authors. Correspondence and requests for materials should be addressed to: wujinrong@scu.edu.cn (J.R. Wu) and liujun@mail.buct.edu.cn (J. Liu)

[a] State Key Laboratory of Polymer Materials Engineering, College of Polymer Science and Engineering, Sichuan University

Chengdu 610065, People's Republic of China

E-mail: wujinrong@scu.edu.cn

[b] State Key Laboratory of Organic-Inorganic Composites, Beijing University of Chemical Technology

Interdisciplinary Research Center for Artificial Intelligence, Beijing University of Chemical Technology

Beijing 100029, People's Republic of China

Email: liujun@mail.buct.edu.cn

Supporting Information

SI Materials and Methods

Table S1-S6

Figures S1-S20

Experimental Section

Materials and Methods

Materials: Materials and agents were obtained from the indicated commercial suppliers and could be used without further purification unless otherwise specified: 2-Hydroxyethyl Methacrylate (HEMA, Adamas, 99%, safe dry), 2-Bromoisobutyryl bromide (BIB) (Adamas, 99%), triethylamine (TEA, Adamas, 99%), anhydrous dichloromethane (DCM, Adamas, 99%, safe dry), methyl methacrylate (MMA, Adamas, 99%), 2,2-Azobis(isobutyronitrile) (AIBN, TCI, 98.0%), ethyl acrylate (EA, TCI, 99.0% (GC)), N,N,N',N'',N''-pentamethyldiethylenetriamine (PMEDTA, TCI, 99.0% (GC)), copper (I) bromide (CuBr) was purified by stirringovernight in acetic acid glacial. More details about the raw materials were shown in Table S1.

Table S1. List of raw materials and agents

Raw materials and agents	abbreviation	purity	producer
Methanol	CH_3OH	99.9%	Adamas
Tetrahydrofuran	THF	99.0%	Greagent
Ethyl acetate	$CH_3COOCH_2CH_3$	99.5%	Greagent
Magnesium sulfate anhydrous	$MgSO_4$	99%	Adamas
Sodium bicarbonate	$NaHCO_3$	99%	Adamas
Hydrochloric acid	HCl	36-38%	Gregent

Synthesis of 2-(2-Bromoisobutyryloxy)ethyl methacrylate (BIEM). BIEM was synthesized referring to literatures.[1] HEMA (80 mmol), TEA (80 mmol), and anhydrous dichloromethane (60 ml) were added to a dry round-bottom flask, the mixture was cooled in an ice bath while stirring, and a solution of 2-BIB (88.0 mmol)

in anhydrous dichloromethane (10 mL) was added dropwise through constant pressure funnel over 30 min under argon atmosphere. The mixed solution was kept cold and stirring overnight to complete the reaction. After at least 24 h, the white precipitate was filtered out and washed with DCM twice, the obtained organic phase was washed three times with 15 wt% HCl solution, 15 wt% NaHCO$_3$ solution and deionized water respectively and then dried with anhydrous MgSO$_4$, and the solvent was removed through rotary evaporator to obtain a pale yellow liquid, which was defined by ^{1}H NMR (Fig.S1).

Synthesis of macroinitiators P(BIEM-co-MMA). The macroinitiators were synthesized by free-radical copolymerization of MMA and BIEM. MMA, BIEM and AIBN were dissolved in toluene in the specified proportion, the solution was bubbled with argon for 30 mins and then heated 70 °C for at least 12 h under argon atmosphere. The resulting solution was precipitated in methanol at least three times, and finally the precipitate was dried at 45 °C in a vacuum oven for at least 48 h. The actual ratio of MMA and BIEM in the copolymer was determined by ^{1}H NMR, and then the number of MMA (n) and BIEM (m) in the copolymer chain was calculated by combining the results of ^{1}H NMR (Fig.S2) and GPC. The details of the macroinitiators were shown in Table S2.

Table S2. Characterization of the backbones.

Samples	The theoretical graft density (BIEM:MMA) [a]	The actual graft density (BIEM:MMA) [b]	Length of side chain	$\overline{M}_n$ g/mol	PDI
BIEM-MMA-1-8	1:8	1:7.1	50	93000	2.6
BIEM-MMA-1-4	1:4	1:3.6	70	50000	2.9
BIEM-MMA-1-2	1:2	1:2	50	90000	4.9
BIEM-MMA-1-1	1:1	1:1.03	50	50000	4.7

[a] The feed ratio of MMA and BIEM when the main chains were synthesized;

[b] The actual molar ratio of MMA and BIEM in the backbones;

Synthesis of bottlebrushes. Bottlebrushes were prepared by atom transfer radical polymerization (ATRP) making use of macroinitiator as initiator. Typically for 4-1-EA-50, the Shrek reaction bottle was used as reaction vessel, macroinitiator-4-1(1 g, 1.05 mmol Br) was dissolved in 10 ml toluene first, and then EA (5.2553 g, 0.0525 mol) and PMEDTA (0.3639 g, 2.10 mmol) were dissolved in another 10 ml toluene, the mixture was cooled in ice bath and bubble with argon for 2 h to remove oxygen in the solution as much as possible, afterwards, CuBr (0.1506 g, 1.05 mmol) was added in the reaction solution quickly and the reaction vessel was sealed, thereafter the mixture was heated 70 °C for 4 h under argon atmosphere. After the reaction, THF was added into the reaction solution to cool it down to room temperature rapidly, the product was filtered through a plug of neutral alumina oxide to remove most of Cu^{2+} and Cu^+, and THF was used as eluent. After filtering, THF was removed through rotary evaporator at 35 °C, then the resulting solution was precipitated in the mixed solvent of methanol and deionized water (3:1) at least three times. The precipitate was dried at 35 °C in a vacuum oven for at least 48 h finally. The details of the bottlebrushes were shown in Table S3.

Table S3. Characterization of bottlebrushes.

Samples	The theoretical graft density (BIEM:MMA) [a]	The actual graft density (BIEM:MMA) [b]	Length of side chain
1-8-EA-50	1:8	1:7.1	50
1-4-EA-70	1:4	1:3.6	70
1-4-EA-50	1:4	1:3.6	50
1-4-EA-20	1:4	1:3.6	20
1-2-EA-50	1:2	1:2	50
1-1-EA-50	1:1	1:1.03	50

[a] The feed ratio of MMA and BIEM when the main chains were synthesized;

[b] The actual molar ratio of MMA and BIEM in the backbones;

Simulation method

In order to establish the relationship between the microstructure and macroscopic properties of the bottlebrush polymer more profoundly, we constructed a coarse-grained model including the backbone and side chain according to the experiment by using molecular dynamics (MD) simulations, as shown in Fig.1(b).Two structural parameters corresponding to the experiment were probed, including (1) Grafting density of side chains $m/(m+n)$, and (2) side chain length z. Fig.1 (b) also provides a snapshot of the equilibrium state of the system with $n=m=1$, $z=20$.

The coarse-grained model adopted is a variant of the Kremer and Grest standard bead-spring model,[2] which is frequently used to study complex large-scale polymer systems.[3] The nonbonded interactions between all beads are described by the truncated and shifted Lennard-Jones (LJ) potential:

$$U(r) = \begin{cases} 4\varepsilon \left[\left(\dfrac{\sigma}{r-\Delta} \right)^{12} - \left(\dfrac{\sigma}{r-\Delta} \right)^{6} \right] + C & r < r_{cutoff} + \Delta \\ 0 & r \geq r_{cutoff} + \Delta \end{cases} \tag{1}$$

where σ defines the length scale and ε is the pair interaction energy parameter. The value of the interaction strength (ε) is about 2.5-4.2 kJ/mol for different polymers when mapping the bead-spring model to the real polymers. Δ is considered as the effect of the excluded volume of different interaction sites. Therefore, Δ is set with different values according to different pair beads with specific diameters, and the real cutoff distance is the sum of r_{cutoff} and Δ. C is a constant to maintain the continuity of the equation. The attractive or repulsive interactions have been modeled by the different values of r_{cutoff}. Based on the experiments, we consider the backbone and side chains as two types of polymers and use the conventional force field: attractive potentials are set between the same components ($r_{cutoff} = 2.24\sigma$); repulsive potentials are set between different components ($r_{cutoff} = 2^{1/6}\sigma$). Compared to PEA, the molecular chain of PMMA has extremely high rigidity and spatial resistance, so the diameters of the

backbone beads (type A) and side chain beads are set to 3σ and 1σ, respectively. The detailed parameters include the interaction strength and the cutoff radius are shown in Table S4.

Table S4. Interaction potential energy parameters between components

Nonbonded pair		Δ/σ	$\varepsilon_{ij}/\varepsilon$	r_{cutoff}/σ
Backbone (type A)	Backbone (type A)	2	1.0	2.24
Backbone (type A)	Side chain (type B)	1	1.0	1.12
Side chain (type B)	Side chain (type B)	0	1.0	2.24

The bond interactions between the adjacent beads are modelled by a harmonic potential:[4]

$$U_{bond} = \frac{1}{2}K\left(r - r_0\right)^2 \qquad (2)$$

where K is the bond strength constant, $K = 200$; r_0 is the equilibrium bond distance between adjacent beads. The harmonic potential was proved to be efficient in modelling polymer chains.[5]

The bending angle of the polymer chain between three consecutive beads was modeled by a harmonic potential:

$$U_{angle} = \frac{1}{2}k\left(\theta - \theta_0\right)^2 \qquad (3)$$

where k denotes the chain stiffness and θ_0 is the equilibrium value of the angle. The k of the backbone and side chain were set to 15 and 10, respectively, to better correspond to the experiment.

Based on the experiments, we also designed the corresponding systems to investigate the effects of side chain length and graft density on the mechanical properties and self-healing properties of the materials. Here, we fix m to 1 and regulate the grafting density of the side chains by varying n to 1, 2 and 3, corresponding to three systems (systems 1-1-20, 1-2-20, and 1-3-20), where the chain length z is fixed to 20. When exploring the effect of side-chain length, we kept the graft density constant at 1-1 and changed the side chain length z to 10, 15, 20, 40, and 60. Moreover, the number

of A beads per chain, N_A, is fixed around 50, and the number of B beads, N_B, varies

with n and z. Specific structural parameters of each system are shown in Table S5.

Table S5. Structural Parameters of Different Systems

systems	m	n	Z	N_A	N_B
1-1-10	1	1	10	50	500
1-1-15	1	1	15	50	750
1-1-20	1	1	20	50	1000
1-1-40	1	1	40	50	2000
1-1-60	1	1	60	50	3000
1-2-20	1	2	20	50	500
1-3-20	1	3	20	51	340

In this MD simulation, periodic boundary conditions were implemented in all three

directions to eliminate edge effects in the simulations. The equations of motion are

integrated using the velocity-Verlet algorithm with a time step $\Delta t = 0.001\tau$, where τ

denotes the LJ time unit $\tau = (m\sigma^2/\varepsilon)^{1/2}$. At the initial stage, the 50 molecular chains

were sequentially arranged in a 500 × 500 × 500 cube simulation box. Then, each

system was annealed under an NVT ensemble with temperature $T^* = 2.0$ for $3 \times 10^3\ \tau$

to eliminate the initial arrangement. The system was then equilibrated for $3 \times 10^3\ \tau$ with

temperature $T^* = 1.5$ under the NVT ensemble. Finally, an NPT ensemble with T* =

1.5 and $P^* = 1.0$ for $11 \times 10^3\ \tau$ was adopted to ensure adequate equilibration. Taking

system 2 as an example, the final number density is around 0.54 and the mass density

is around 0.88. Glass transition temperature (T_g) is around 0.86, so the polymers are in

a melt with $T^* = 1.5$. Fig. S3 illustrates the variation of non-bond energy, temperature

and volume of the 1-1-20 system to reach the final thermodynamic equilibrium state.

After sufficient equilibrium, uniaxial tensile deformation was performed to obtain

the stress-strain curves. The simulation box was stretched in the X direction at a

constant engineering strain rate, while the lengths in the Y and Z directions were

decreased to keep the volume of the simulation box constant. The strain rate was

specified as $\varepsilon_1 = \Delta L / \Delta t = \dfrac{L(t)_X - L_X}{L_X} \Big/ \Delta t = 0.0327 / \tau$, where $L(t)_X$ and L_X were the box length in the X direction at time t and at the beginning, respectively, which is the same as the simulation work from Gao et al. [6] The average stress σ_1 in the Z direction was obtained from the deviatoric part of the stress tensor $\sigma_1 = (1 + \mu)(-P_{XX} + P) \approx 3(-P_{XX} + P)/2$,[7] where $P = \sum_i P_{ii} \Big/ 3$ was the hydrostatic pressure. The parameter μ stands for Poisson's ratio, which was equal to 0.5 here.

For the simulation of self-healing, triaxial stretching was considered as an effective method in the simulation. The triaxial tensile test is generally used to investigate the toughness of the elastomer, which can induce cavitation, crazing, and fracture of the polymer.[8] We can integrate the triaxial stress-strain curve to obtain the dissipated work so as to quantitatively compute the self-healing efficiency.[9] During the deformation, only the X direction of the strain tensor is nonzero, and the box dimensions in the two perpendicular directions remain unchanged, which results in a positive effective stress in all directions.[10] The tensile rate is set to $\varepsilon_2 = 0.0327 / \tau$, which was exactly the same as that of the uniaxial tensile deformation process. The average tensile stress σ in the X direction was obtained from the deviatoric tensor $\sigma_2 = -P_{XX}$, which is the hydrostatic pressure in the X direction. After performing the initial triaxial tension and recovery, the microstructure and intermolecular interactions of the system were still disrupted. Therefore, a range of healing conditions such as the healing temperature and the healing time were applied to the system. Moreover, the self-healing efficiency was defined as $\eta = W_a / W_0 \times 100\%$, where W_0 is and W_a is the tensile dissipation work in the original state and after self-healing, respectively, which is consistent with the experimental definition.

Measurements and methods

Proton nuclear magnetic resonance (^{1}H NMR): ^{1}H NMR were recorded by a Bruker AV III HD 400 MHz spectrometer, and the solvent was CDCl$_3$ (δ (^{1}H) = 7.26 ppm).

Gel permeation chromatography (GPC): The molecular weight was measured by a Tosoh HIC-8320GPC with tetrahydrofuran (THF) as the eluent.

Differential scanning calorimetry (DSC): The heat flow curves of brush-like elastomers were acquired on the Q2000 (TA instruments). The sample was firstly heated from 25 ℃ to 60 ℃ and then cooled from 60 ℃ to -70 ℃ with the rate of 20 ℃/min to eliminate thermal history, and then the sample was heated from -70 ℃ to 60 ℃ with the rate of 10 ℃/min to record the heat flow. The glass transition temperature (T_g) of the samples were defined as the inflection point of the heating curves.

Rheology: The rheological measurements were carried out by the HAAKE MARS (Mars III). Temperature sweeping from 25 ℃ to 140 ℃ was performed with the strain of 1% and the constant frequency of 1 Hz under the heating rate of 10 ℃/min.

Tensile test: Tensile experiments were performed on an Instron 5967 tensile tester. Samples were cut into the dumbbell shape by a normalized cutter with the gauge length of 20 mm, the width of 2 mm and the thickness of 0.5-1 mm. Uniaxial tensile measurements were performed at room temperature in the air with the strain rate of 80 mm/min. The Young's modulus was determined by the slope within the initial linear region of the stress-strain curves.

Dynamic Mechanical Analysis (DMA): Dynamic mechanical properties were measured on the Q800 (TA instruments) in the tension mode. The geometry rectangular samples were heated from -70 ℃ to 100 ℃ with the heating rate of 5 ℃/min, the frequency of 1 Hz and the preload force of 0.01 N.

Drop hammer impact tests: The impulse signals (the impulse force) of the materials with 1 mm is produced by an impact hammer and the impulse force is in the range of 30–35N. The response signals are collected by the acceleration sensor.

Shaking table demonstrative experiments: The acceleration sensors is placed on the shaking table and materials, respectively. They are all submitted to a sinusoidal longitudinal vibration of 670 kHz frequency and collected response signals.

Primitive path analysis of entanglement length: The primitive path analysis (PPA) proposed by Everaers et al.,[11] which is based on the concept of Edwards's tube model,[12] was employed to identify the primitive path of each strand. To obtain a mesh of primitive paths in simulations, first, the chain ends are fixed in space. Then, the intrachain excluded-volume interactions are disabled, while retaining the interchain excluded-volume interactions. Finally the energy of the system is minimized by slowly cooling the system toward $T^* = 0.001\varepsilon/kB$ (close to zero). Without thermal fluctuations and intrachain excluded-volume interactions, the bond springs try to reduce the bond length to zero and pull the chains taut. The interchain excluded-volume interactions ensure that different chains do not cut through each other, and thus the topology is conserved throughout the procedure. Such stretched conformations of chains then can be considered as the primitive paths of the initial chains, and hence their mean square end-to-end distance remains the same, i.e., $\left\langle R_e^2(N) \right\rangle = l_k^{(pp)} L_{pp} = l_k^{(pp)}(N-1)l_b^{(pp)}$, and $l_k^{(pp)}$ where L_{pp}, $l_b^{(pp)}$ and N are the Kuhn length, contour length, average bond length of the primitive path and number of monomers per chain. The so-called entanglement length N_e defined by the number of monomers per Kuhn segment of the primitive path is then $N_e = l_k^{(pp)} / l_b^{(pp)}$. Therefore, the number of entanglement points in each chain can be calculated by N_e,

$$\left\langle Z \right\rangle = N/N_e - 1.$$

Theoretical Calculation

Self-healing efficiency (η): Healing efficiency (η) is calculated according to the following equation (1):

$$\eta = \frac{U_T^{heal}}{U_T^{uncut}} *100\% \tag{1}$$

Where U_T^{heal} refers to the strain energy density of samples after repaired, and U_T^{uncut} refers to the strain energy density of the original samples without cutting.

True stress: The true stress can be calculated by the following equation (2):

$$\sigma_{true} = (1 + \varepsilon)\sigma \tag{2}$$

Where σ refers to stress and ε refers to strain.

dissipation efficiency (η_d): The dissipation efficiency is calculated by the following equation:

(3)

$$\eta_d = \frac{A_0 - A_1}{A_0} \times 100\%$$

Where A_0 represents the amplitude of acceleration signals on the shaking table, A_1 represents the amplitude of acceleration signals on the damping rubbers.

Figures and Tables
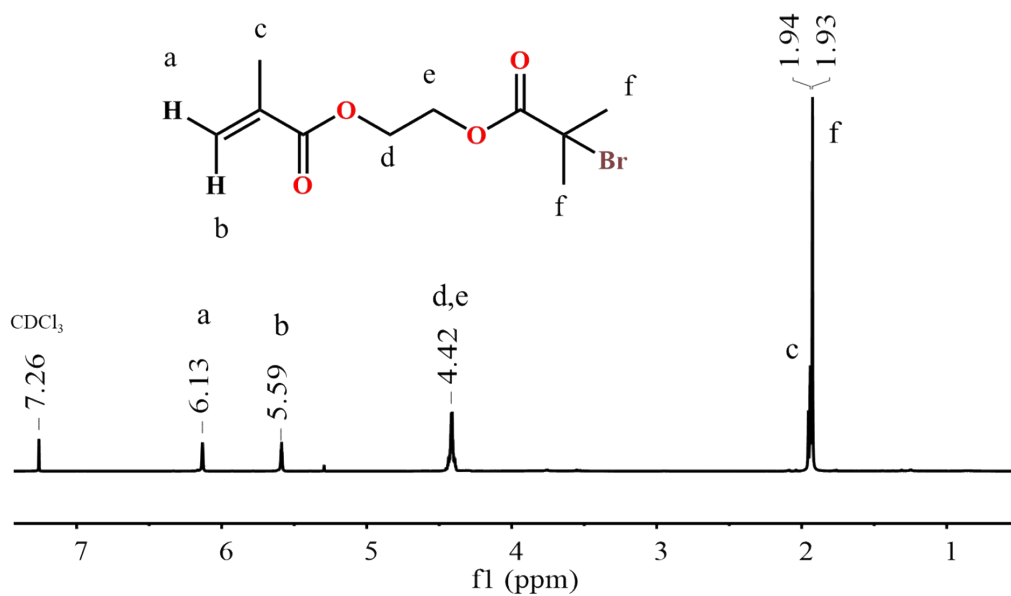
Fig.S1. The ^{1}H NMR spectra of BIEM (400 MHz, CDCl$_3$).
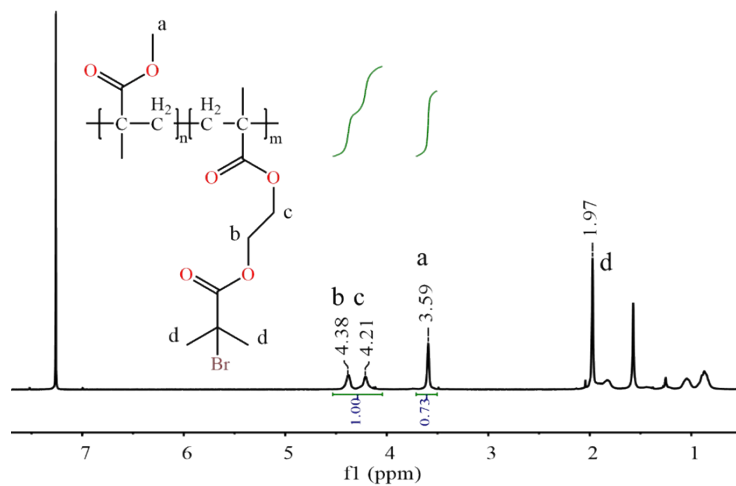
Fig.S2. The ^{1}H NMR spectra of P(BIEM-*co*-MMA)-1-1 (400 MHz, CDCl$_3$):

m(BIEM)/n(MMA)=(area(b+c)/4)/(area(a)/3) =1:1.03
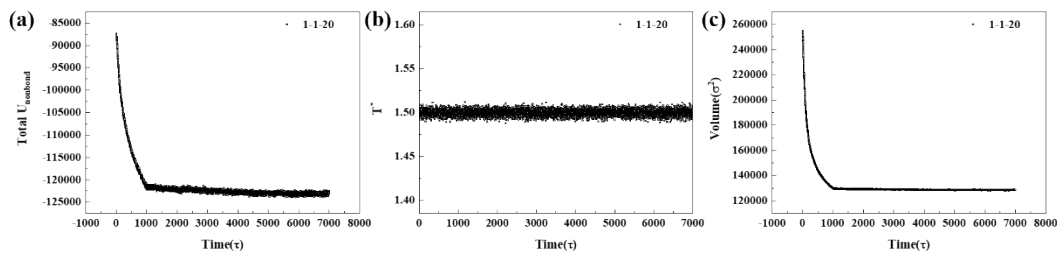
Fig. S3. The 1-1-20 system is used as an example to monitor the (a) total non-bond energy, (b) temperature and (c) volume during equilibrium.
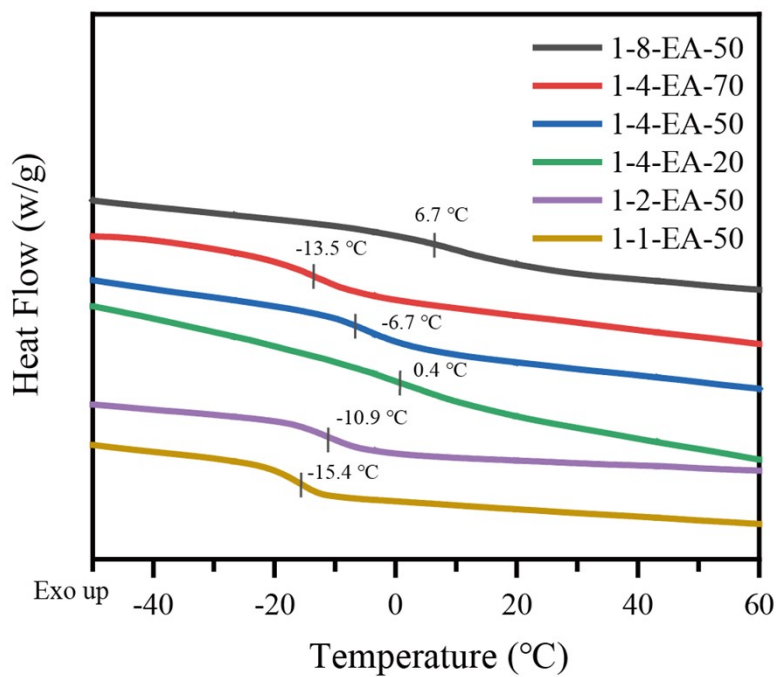
Fig.S4. The DSC curves of bottle-brush polymers.
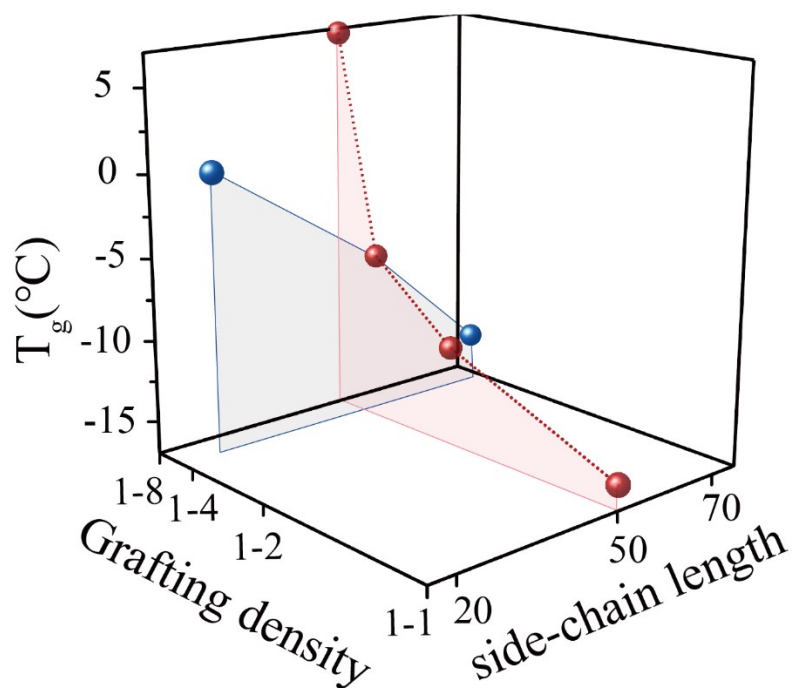
Fig.S5. Comparing the T_g of samples with different grafting density and side-chain length.
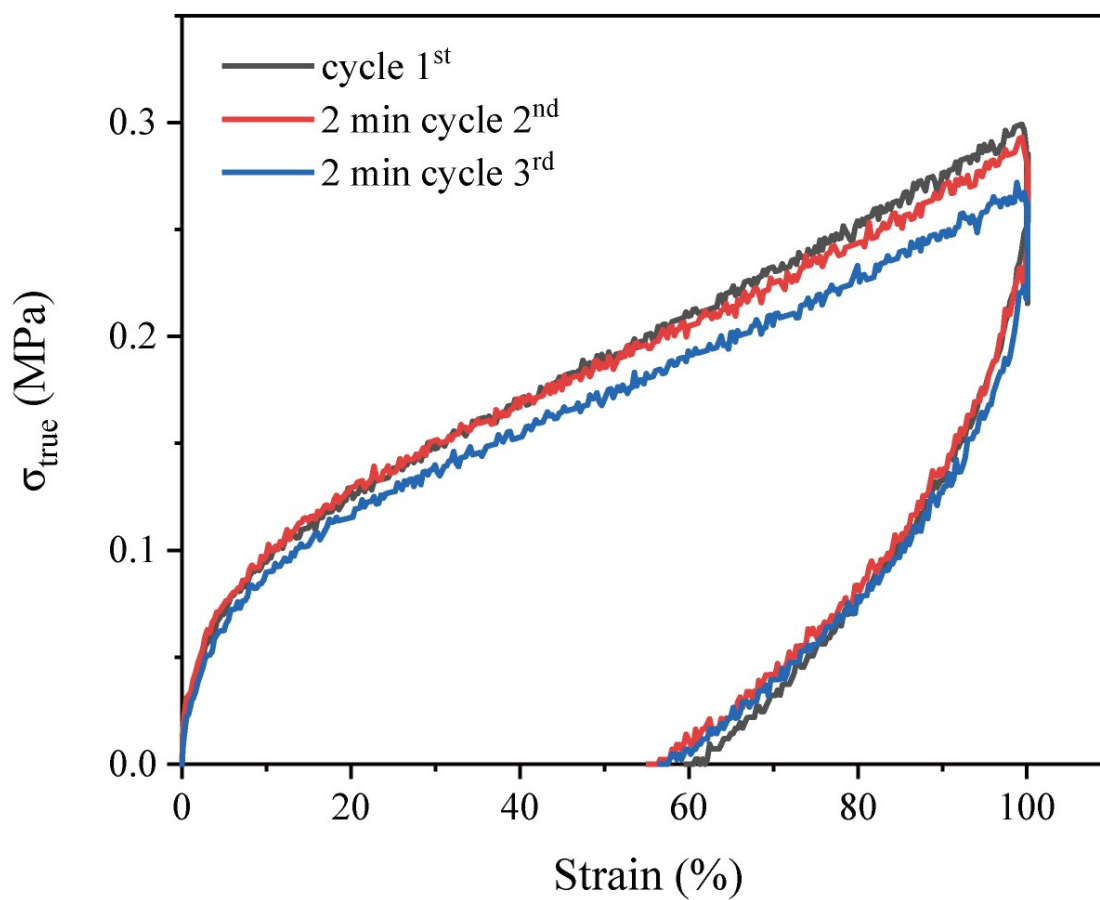
Fig.S6. Load-unload cycling curves of 1-4-EA-50 sample under 100% strain for 2 min

relaxation times.
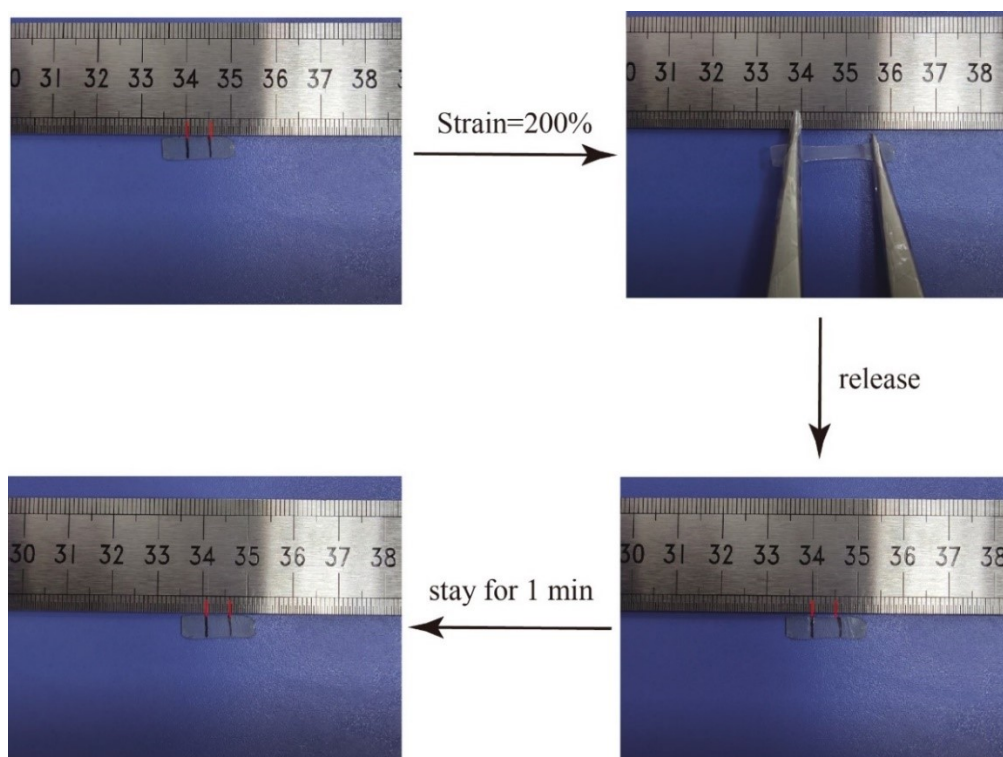
Fig.S7. The length recovery process of 1-4-EA-50 after stretching the sample to 200% strain. After 1 min, the length completely restored.
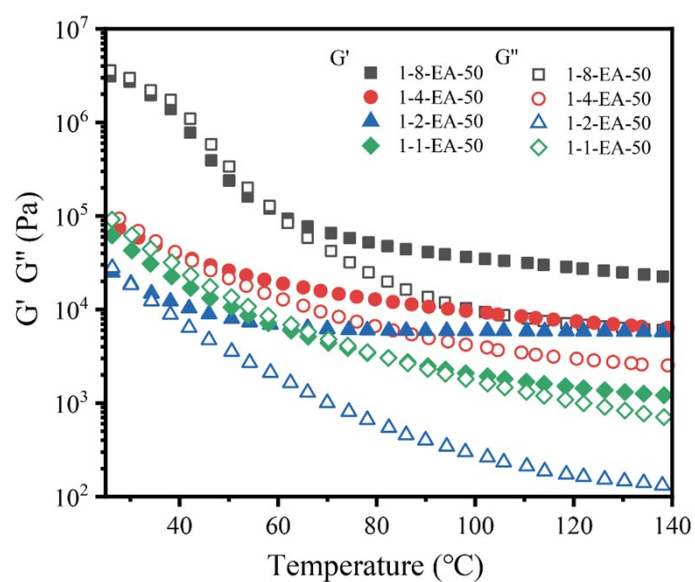
Fig. S8. The results of rheological tests using the temperatures weeping mode under the heating/cooling rate of 10 °C/min with the strain of 1% and the constant frequency of 1 Hz. The storage modulus (G') (solid) and loss modulus (G'') (open) of 1-8-EA-50 (square), 1-4-EA-50 (circle), 1-2-EA-50 (triangle), 1-1-EA-50 (rhombus).
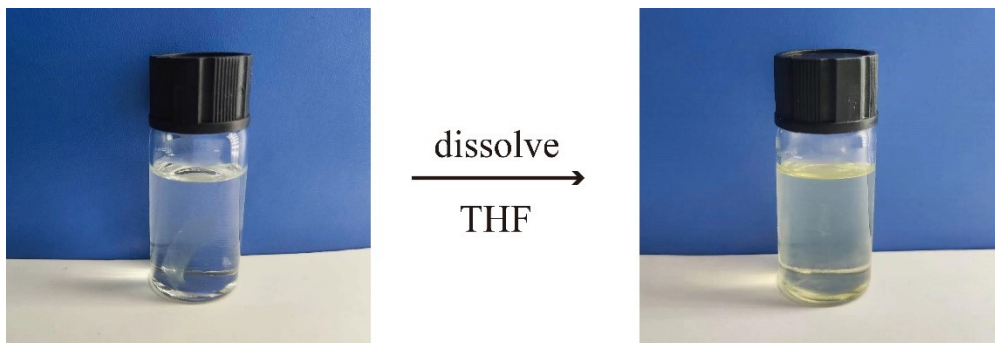
Fig. S9. Sample 1-4-EA-50 can completely dissolve in THF
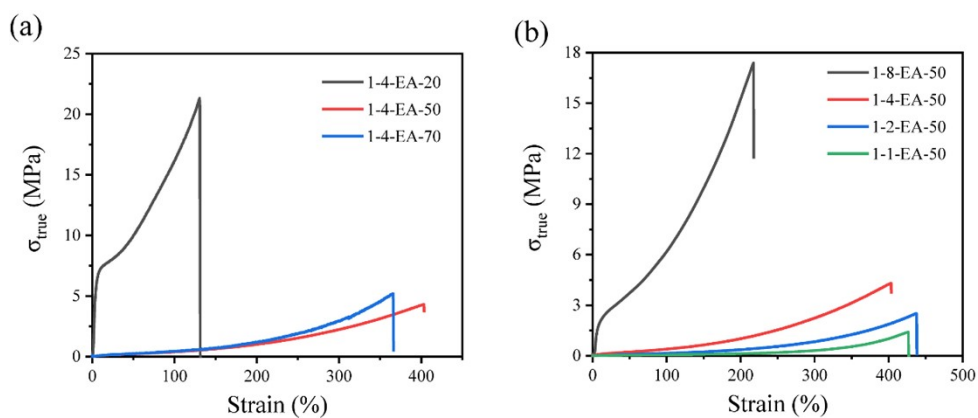
Fig.S10 Representative stress-strain curves of sample **(a)** 1-4-EA-20, 1-4-EA-50, 1-4-EA-70 with different side-chain length and **(b)** 1-8-EA-50, 1-4-EA-50, 1- 2-EA-50 and 1-1-EA-50 with different grafting density at the tensile rate of 100 mm/min.
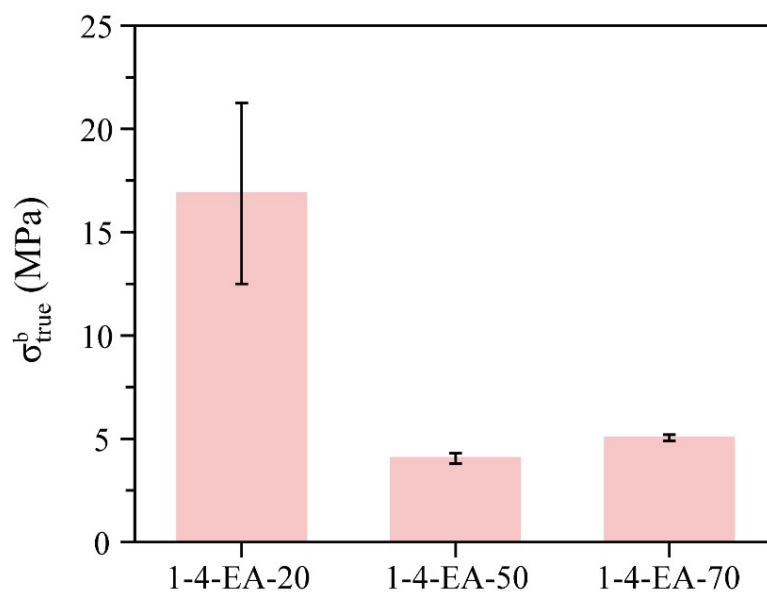
Fig.S11 σ_{true}^{b} comparison of samples with different grafting density and side-chain length.

Table S6. Mechanical properties of bottlebrushes

Samples	True stress at break (σ^b_{true})	Young's Modulus
1-8-EA-50	16.40±1.0	34.6±1.1
1-4-EA-20	16.9±4.2	287.5±9.5
1-4-EA-50	4.1±0.25	1±0.02
1-4-EA-70	5.1±0.15	1.6±0.2
1-2-EA-50	2.7±0.003	0.3±0.01
1-1-EA-50	1.4±0.05	0.1±0.01
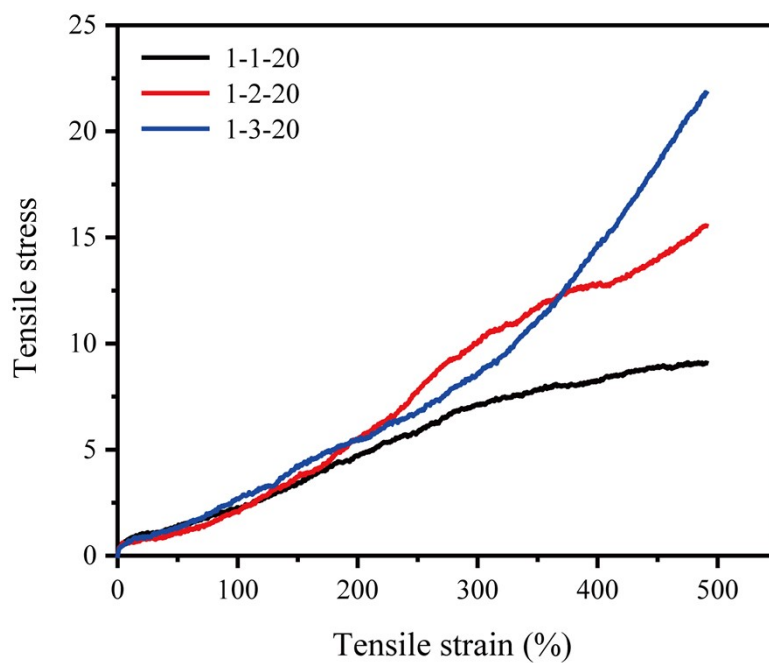
Fig. S12. Stress-strain curves for systems with different grafting densities subjected to uniaxial tension.
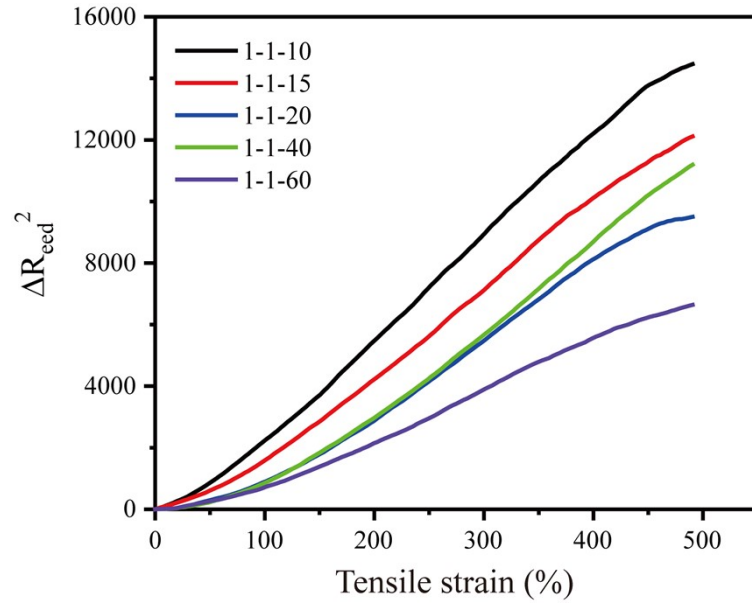
Fig. S13. Evolution of the mean square end distance of the backbone in deformation.

cut   heal at 40 ℃ for 12 h   heal at 40 ℃ for 24 h
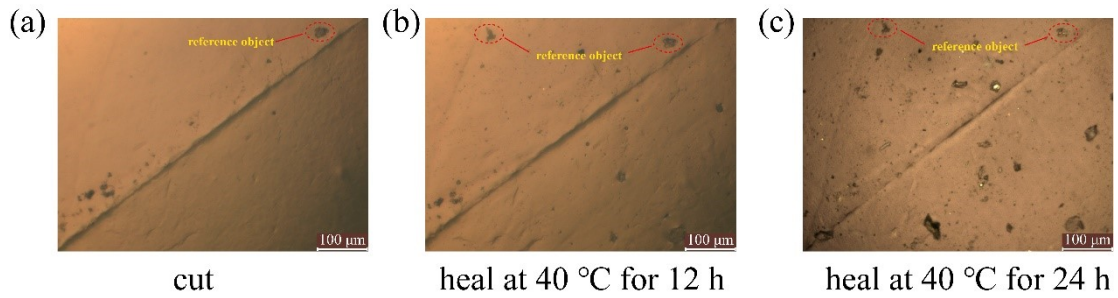
Fig. S14. The scratches can heal at 40 ℃ for 24h
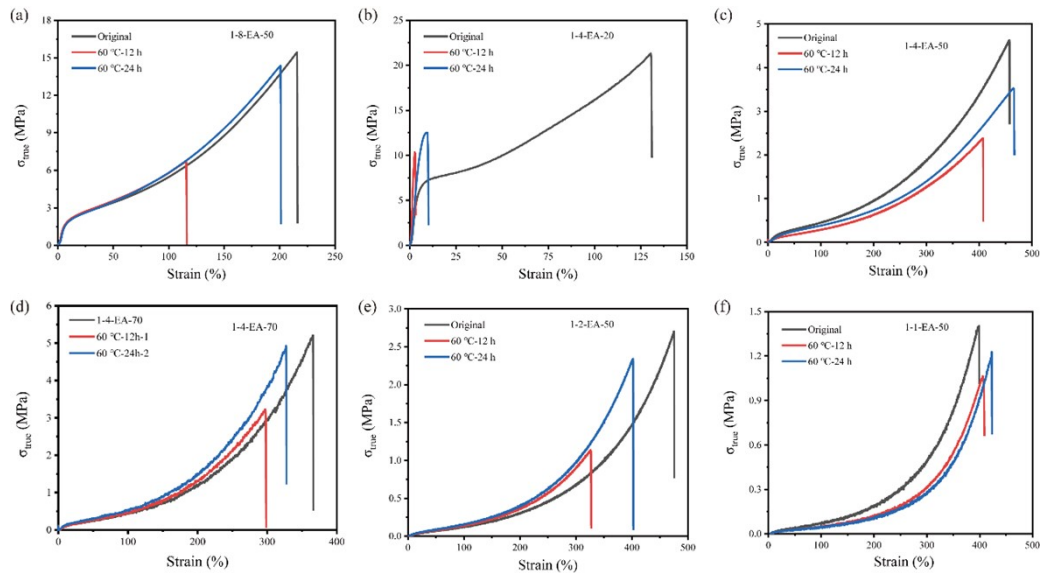
Fig. S15. Representative stress-strain curves of the original samples and the cut samples healed at 60 ℃ for 12 h and 24 h for the samples. (a) 1-8-EA-20; (b) 1-7-EA-20; (c) 1-4-EA-50; (d) 1-4- EA-70; (e) 1-2-EA-50; (f) 1-1-EA-50.
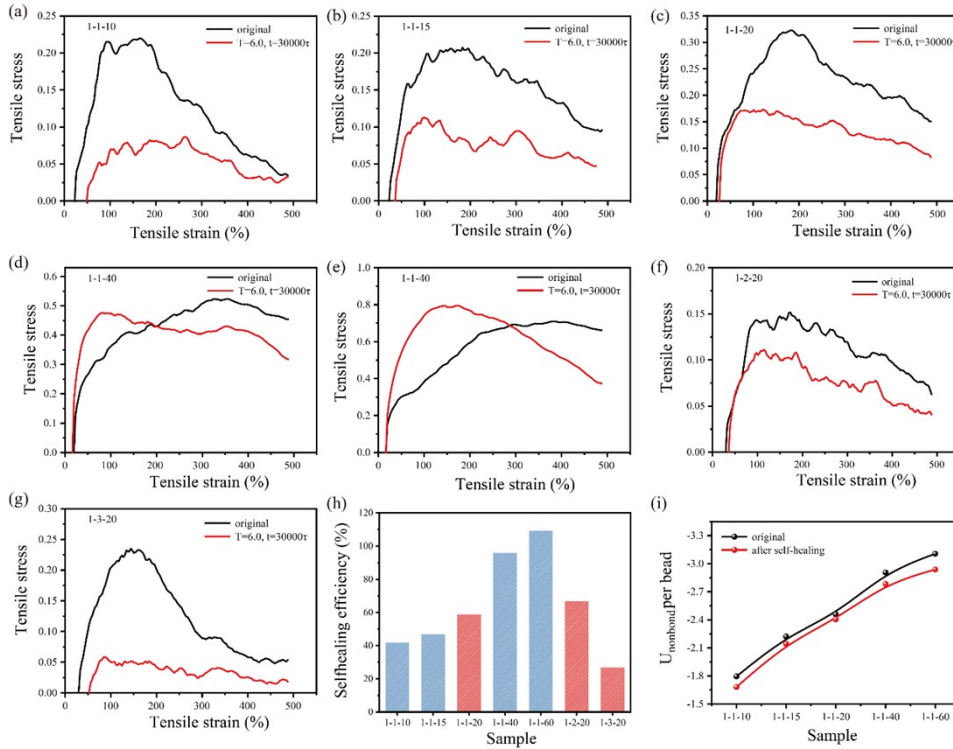
Fig. S16. (a)-(g) Stress-strain behavior of the original and healing samples. (h) self-healing efficiency of systems with various side-chain lengths and grafting densities. (i) Normalized non-bonding energy of side chain beads before and after self-healing for the bottlebrush polymers with different side-chain length.
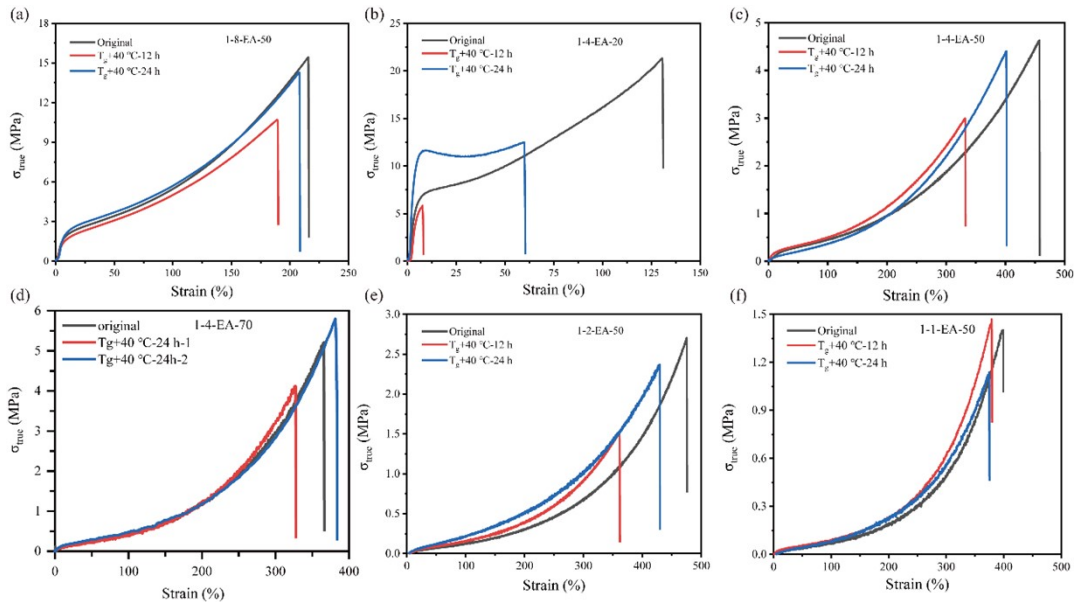
Fig. S17. Representative stress-strain curves of the original samples and the cut samples healed at T_g+40 °C for 12 h and 24 h for (a) 1-8-EA-50; (b) 1-4-EA-20; (c) 1-4-EA-50; (d) 1-4-EA-70; (e) 1-2-EA-50; (f) 1-1-EA-50.
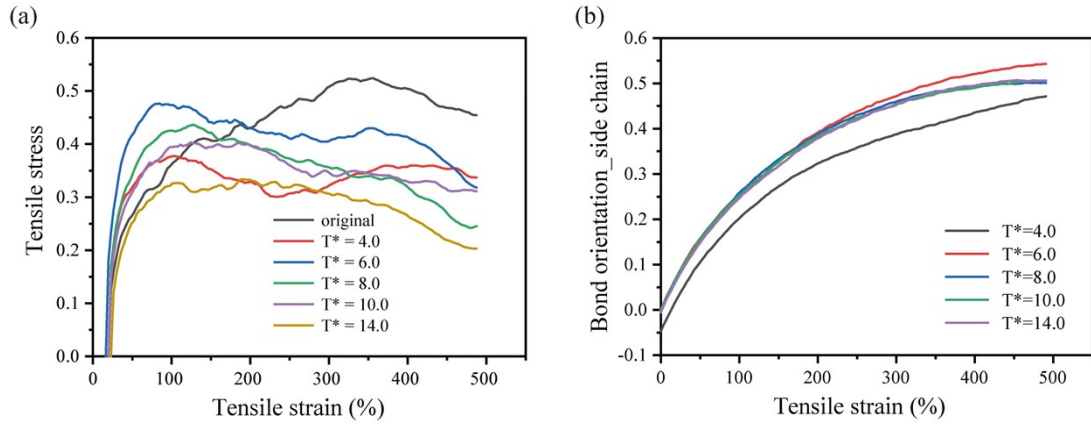
Fig. S18. (a) Stress-strain curves of system 1-1-40 after self-healing at different temperatures with healing time of 30000τ. (b) Bond orientation behavior of side chains during deformation after self-healing at different temperatures.
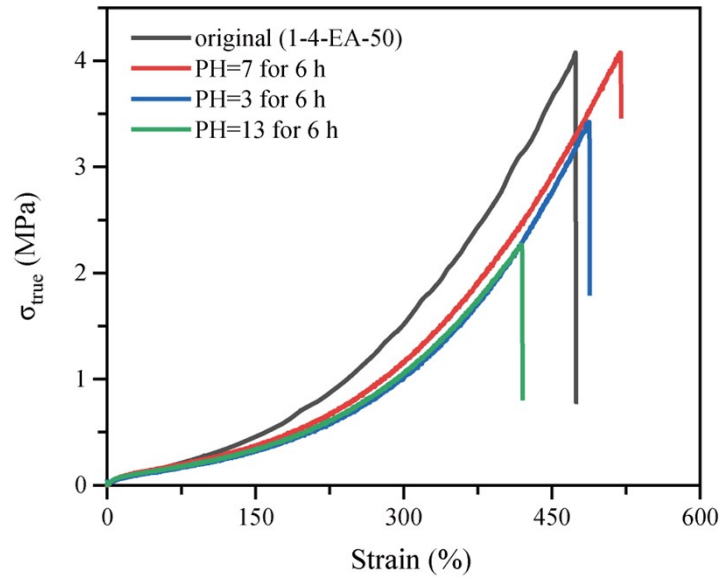
Fig.S19. Stress–strain curve of the cut 1-4-EA-50 healing at Tg+40 °C (35 °C) for 6 h under various harsh conditions.
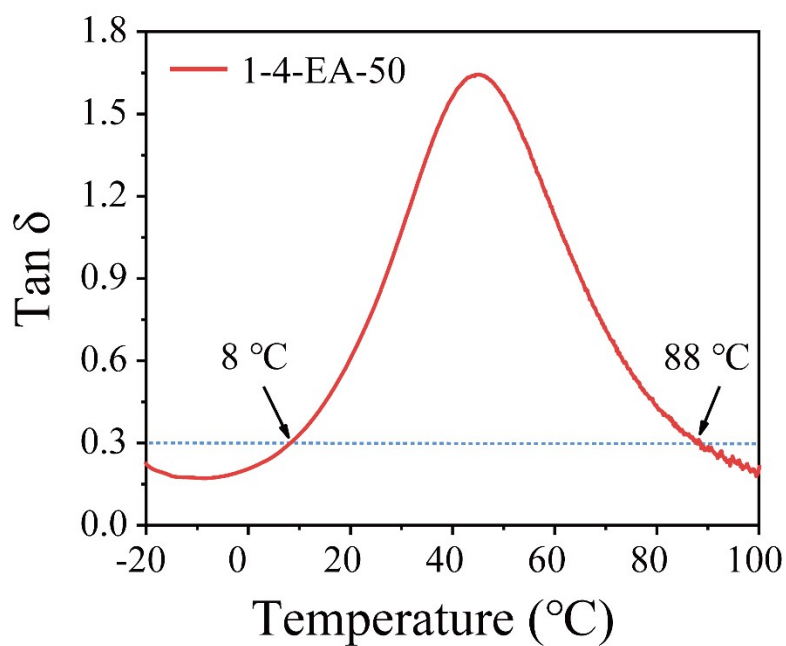
Fig. S20. Temperature-dependent Tanδ tested by DMA.
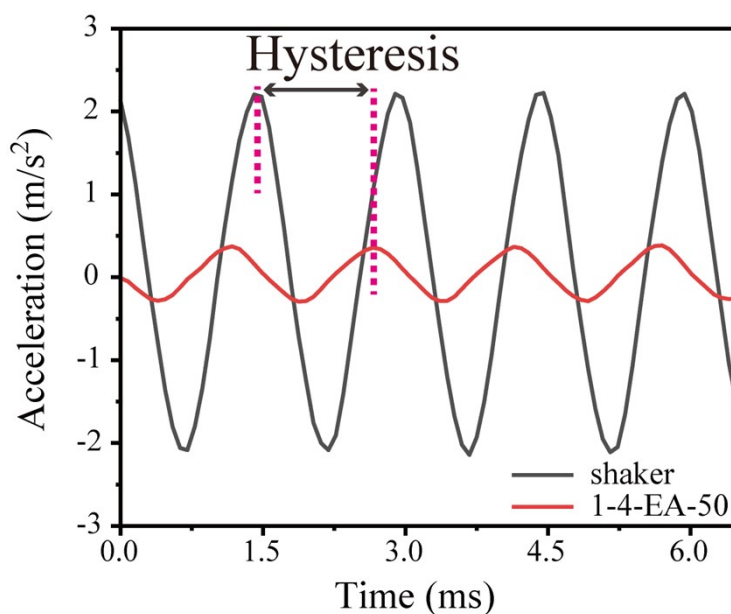
Fig. S21. The signal phase of 1-4-EA-50 possess significant hysteresis.

References

[1] A. M. Hanlon, R. Chen, K. J. Rodriguez, C. Willis, J. G. Dickinson, M. Cashman, E. B. Berda, *Macromolecules* **2017**, 50, 2996.

[2] K. Kremer, G. S. Grest, *The Journal of Chemical Physics* **1990**, 92, 5057.

[3] F. W. Starr, T. B. Schrøder, S. C. Glotzer, *Macromolecules* **2002**, 35, 4481.

[4] G. N. Toepperwein, N. C. Karayiannis, R. A. Riggleman, M. Kroger, J. J. de

Pablo, *Macromolecules* **2011**, 44, 1034.

[5] a)G. Raos, M. Moreno, S. Elli, *Macromolecules* **2006**, 39, 6744; b)G. Srinivas, D. E. Discher, M. L. Klein, *Nature Materials* **2004**, 3, 638; c)Y. Zhang, P. Tiwary, J. S. Parent, M. Kontopoulou, C. B. Park, *Polymer* **2013**, 54, 4814.

[6] J. Ramirez, S. K. Sukumaran, A. E. Likhtman, *J Chem Phys* **2007**, 126, 244904.

[7] R. Everaers, *The European Physical Journal B - Condensed Matter and Complex Systems* **1998**, 4, 341.

[8] a)Z. Zhang, J. Liu, S. Li, K. Gao, V. Ganesan, L. Zhang, *Macromolecules* **2019**, 52, 4154; b)A. R. C. Baljon, M. O. Robbins, *Macromolecules* **2001**, 34, 4200.

[9] Z. Zheng, X. Xia, X. Zeng, X. Li, Y. Wu, J. Liu, L. Zhang, *Macromolecular Rapid Communications* **2018**, 39, 1800382.

[10] J. Liu, J. Shen, Z. Zheng, Y. Wu, L. Zhang, *Nanotechnology* **2015**, 26, 291003.

[11] R. Everaers, S. K. Sukumaran, G. S. Grest, C. Svaneborg, A. Sivasubramanian, K. Kremer, *Science* **2004**, 303, 823.

[12] S. F. Edwards, *P Phys Soc Lond* **1967**, 91, 513.